Electronic Supplementary Material (ESI) for Nanoscale Advances.
This journal is © The Royal Society of Chemistry 2022

Supplementary Information

Photothermal synthesis of CuO_x&FeO_y catalyst with layered double hydroxides-derived pore-confined frame to achieve photothermal CO_2 hydrogenation to CO with a rate of 136 mmol min^{-1} g_{cat}^{-1}

Lizhu Song[a], Xinli Yi[a], Shuxin Ouyang[*,b] , Jinhua Ye[a,c]

[a] *TJU-NIMS International Collaboration Laboratory, School of Materials Science and Engineering, Tianjin University, Tianjin 300072, P. R. China*
[b] *Key Laboratory of Pesticide and Chemical Biology, Ministry of Education, College of Chemistry, Central China Normal University, Wuhan 430079, P. R. China*
[c] *International Center for Materials Nanoarchitectonics (WPI-MANA), National Institute for Materials Science (NIMS), 1-1 Namiki, Tsukuba 305-0047, Japan*

Experimental Section

Synthesis of catalyst precursors：

Typically, 0.38 g $Cu(NO_3)_2 \cdot 3H_2O$, 0.14 g $Fe(NO_3)_3 \cdot 9H_2O$ and 0.5 g LDH ($Mg_6Al_2(CO_3)(OH)_{16} \cdot 4H_2O$) were dissolved in 20 mL deionized water. Then the ethanol (10 mL) was added into the mixture and ultrasound-treated for 5 min to benefit the uniform dispersion of the LDH. All the water was evaporated through a simple evaporation process under magnetic stirring of the heating magnetic stirrer. Then the sample was transferred into a vacuum drying oven and dried at 70^{o}C for 12 h to obtain the final powder. Following the same procedure, the powder samples consist of different components supported by different supports (Al_2O_3, MgO etc.) were synthesized follow the same procedure.

For comparison, the T-CuO_x&FeO_y/MAO catalyst was obtained by calcining the powder in 10% H_2-Ar at 1015^{o}C for 2 h.

Characterizations of catalysts:

The crystal structure was characterized by X-ray diffractometer (D/max-2500, Rigaku, Japan). The light adsorption properties of the catalysts were measured by Ultraviolet-visible (UV-Vis) spectroscopy (UV-2700, Shimadzu, Japan). The microstructure of the catalyst was performed on Scanning electron microscopy (SEM, Quanta FEG 250) and Transmission electron microscopy (TEM, JEM-F200). The spatial distribution of element was confirmed by energy-dispersive X-ray spectroscopy (EDS). The chemical valence state of the element was measured by Xray photoelectron spectroscopy (XPS, Escalab 250Xi, Thermo Fisher Scientific, England). Fourier transform infrared spectroscopy (FT-IR) was recorded by Nicolet 6700 Fourier transform instrument. The Brunauer-Emmett-Teller (BET) surface area and pore structure of the catalyst were analyzed by BET surface area measurement (Autosorb IQ2, Quantachrome, U.S.A.). The temperature of the catalyst surface was measured by a thermocouple (DT-311N).

Activity evaluation:

The reverse water gas shift (RWGS) reaction was carried out in a flow-type photothermal reactor. The process was as follows: 30 mg of the catalyst powder was spread onto a round shape air-permeable quartz fiber filter that was fixed on the sample stage of the reactor. The reaction gases of H_2 and CO_2 (the molar ratio of H_2: CO_2 = 1: 1) were injected into the reactor and the total flowrate was 400.0 mL min^{-1}. A 300 W Xe lamp (CEL-HXF300, CEAULIGHT) equipped with a quartz convergent lens group (FF50Q, MEIWO) was used as the light source, the power of the incident irradiation was 41.3 W (1.42 W/cm^2). The focused irradiation areas of Xe lamp with and without quartz convergent lens group were 29.09 and 0.95 cm^2, respectively. Thus, the irradiation intensity was 439.4 kW m^{-2} (439.4 suns) over catalyst surface. The gas products were detected by gas chromatography (GC-2014C, Shimadzu Co., Japan) equipped with a Paropak Q chromatographic column, a flame ionization detector (FID) and a methanizer. The flow rates of the gas products were measured by a soap flowmeter. The temperature of the catalyst surface was measured using a digital thermocouple (CUSTOM CT-1200D).

The calculations of gas conversion and generation rates:

$$CO_2(\%) = \frac{Inlet(CO_2) - outlet(CO_2)}{Inlet(CO_2)} \times 100\% \quad (1)$$

$$r(CO) = \frac{c(CO) * F}{m} \quad (2)$$

$$Sel(CO) = \frac{m * r(CO)}{Inlet(CO_2) - outlet(CO_2)} \times 100\% \quad (3)$$

Where $CO_2(\%)$ represents the conversion of CO_2, *Inlet(CO_2)* and *Outlet(CO_2)* represent the flow rate of CO_2 at the inlet and outlet; *r(CO)* represents the generation rates of CO*, F* represents the total flow rate of the products, *c(CO)* represents the mole percent of CO in it, *m* represents the mass of the catalyst; $Sel(CO)$ represent the selectivity of CO, respectively.

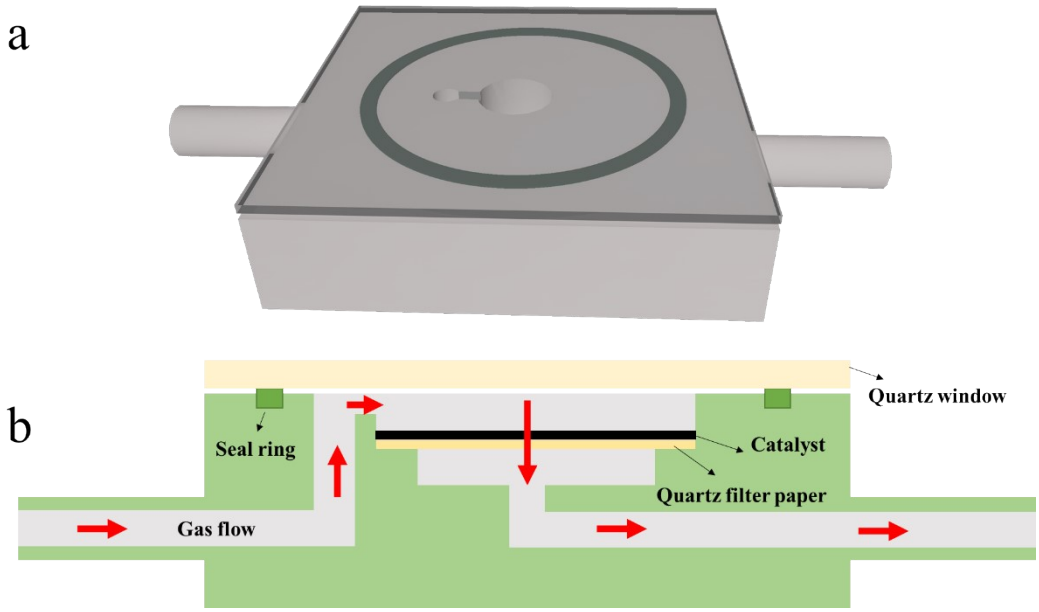

Fig. S1. a 3-D model illustration and **b** illustrated scheme of the flow-type reactor.

Table S1. Specific surface area of the catalyst before and after reaction.

CuO_x&FeO_y/MAO	S_{BET} ($m^2\ g^{-1}$)	Pore volume ($cm^3\ g^{-1}$)	Average pore size (nm)
Before reaction	12.4	0.030	2.769
After reaction	34.9	0.070	3.627

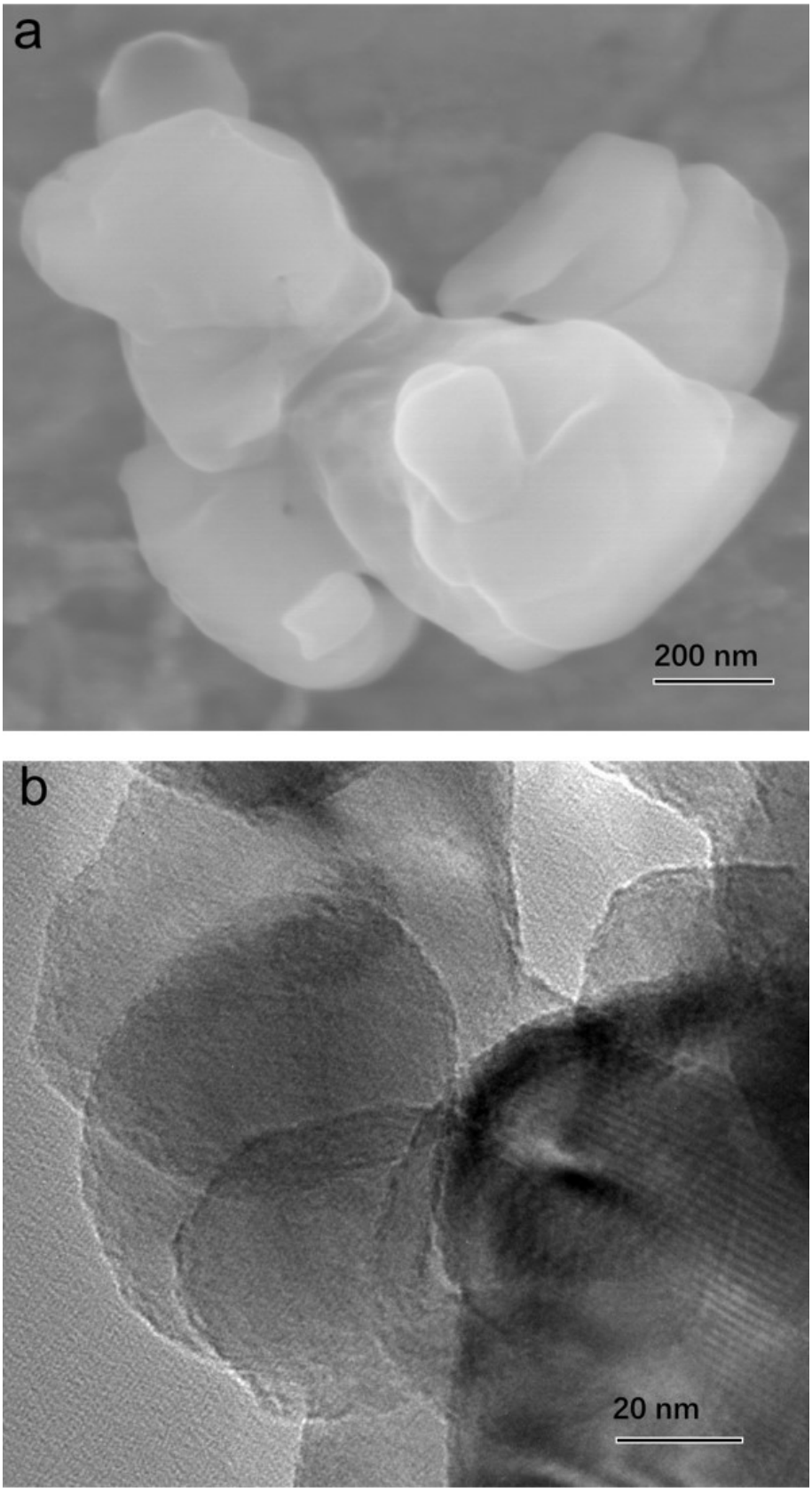

Fig. S2. a SEM image and **b** TEM image of LDH.

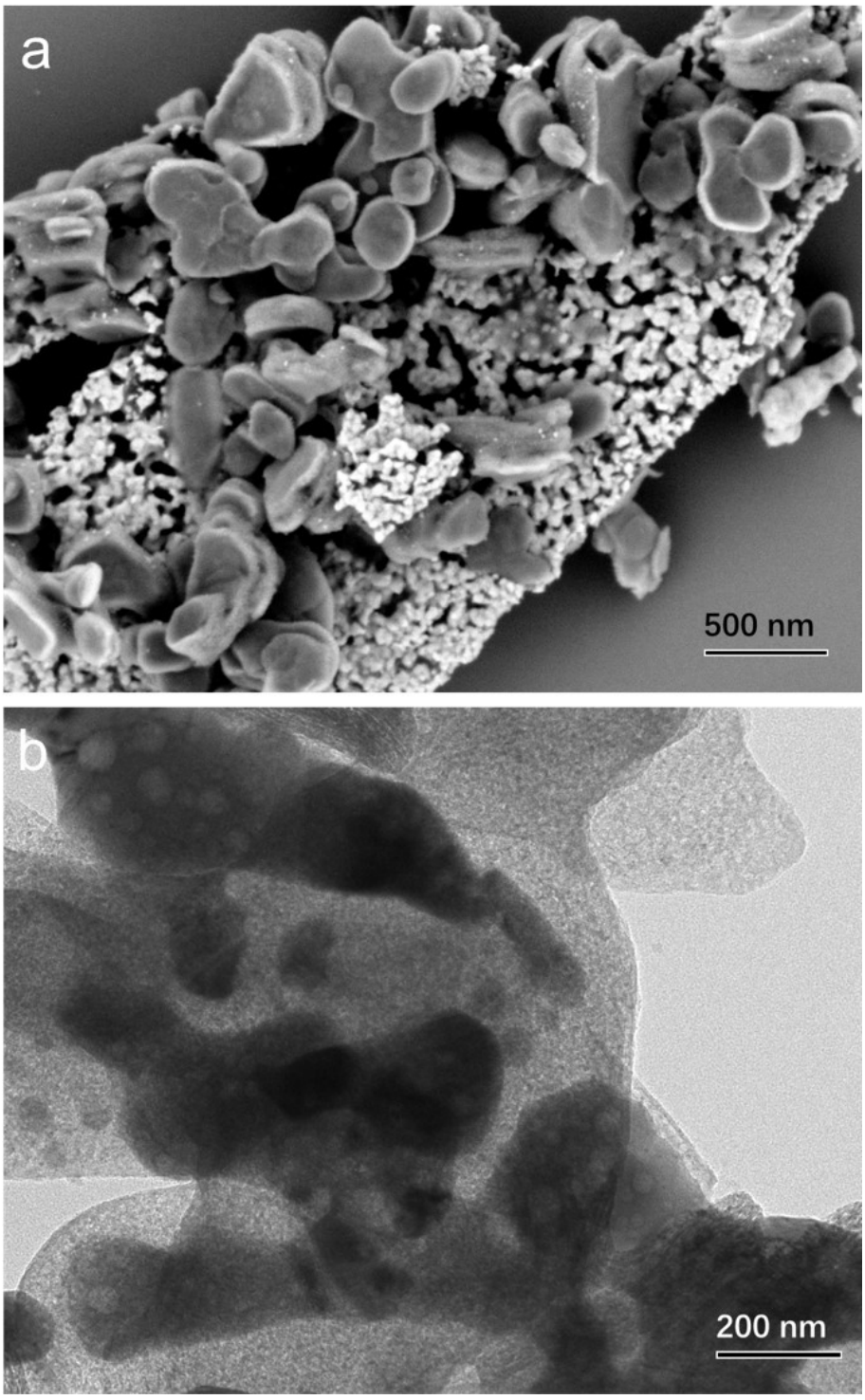

Fig. S3. a SEM image and **b** TEM image of CuO_x/MAO after RWGS reaction.

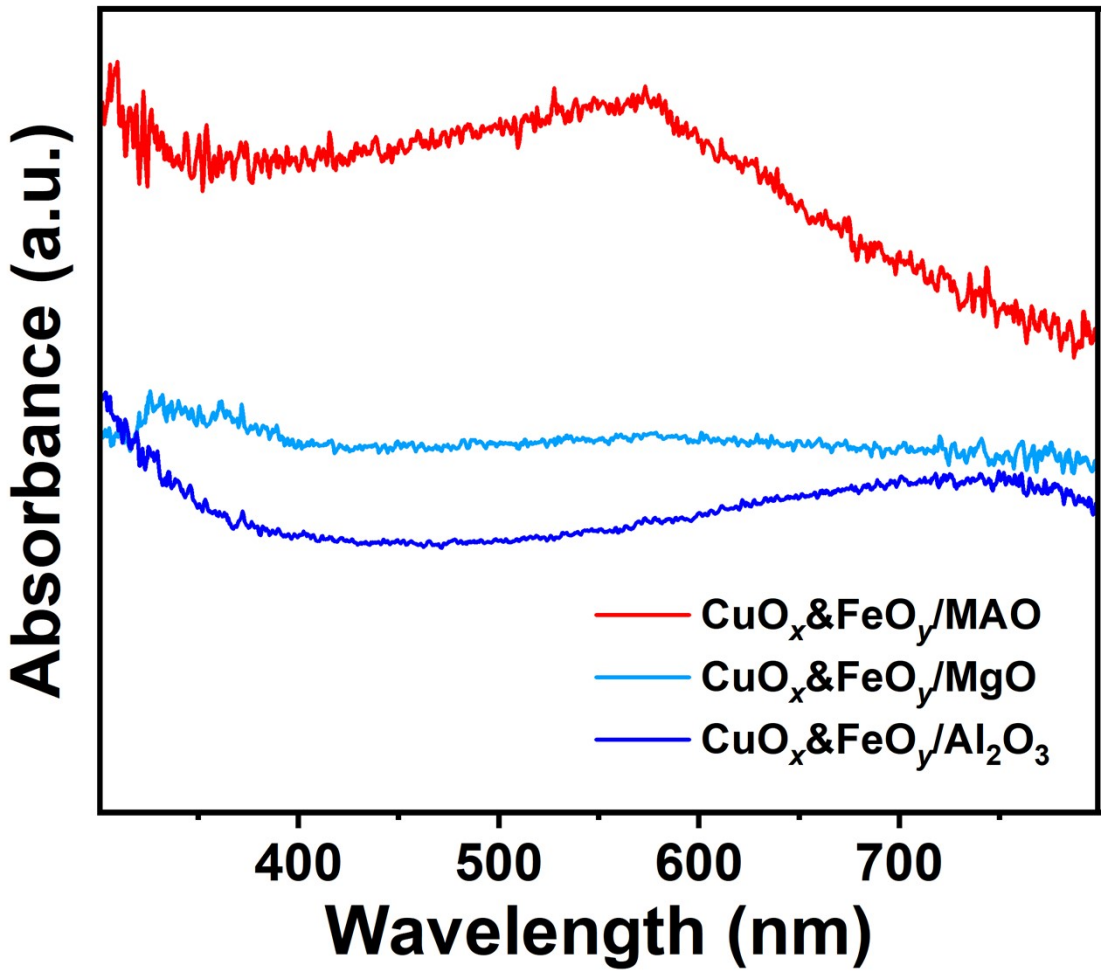

Fig. S4. UV-Vis absorption spectra of the catalysts after RWGS reaction.

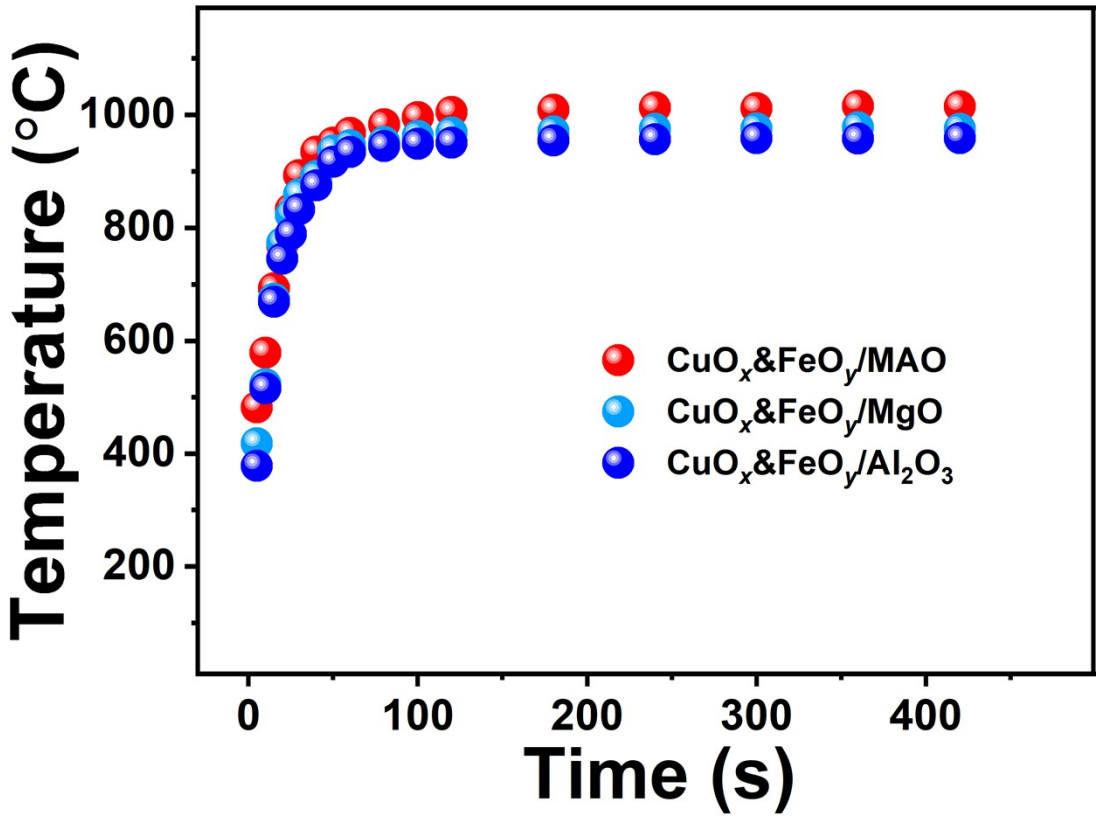

Fig. S5. Temperature variation curves of the catalysts during the reaction.

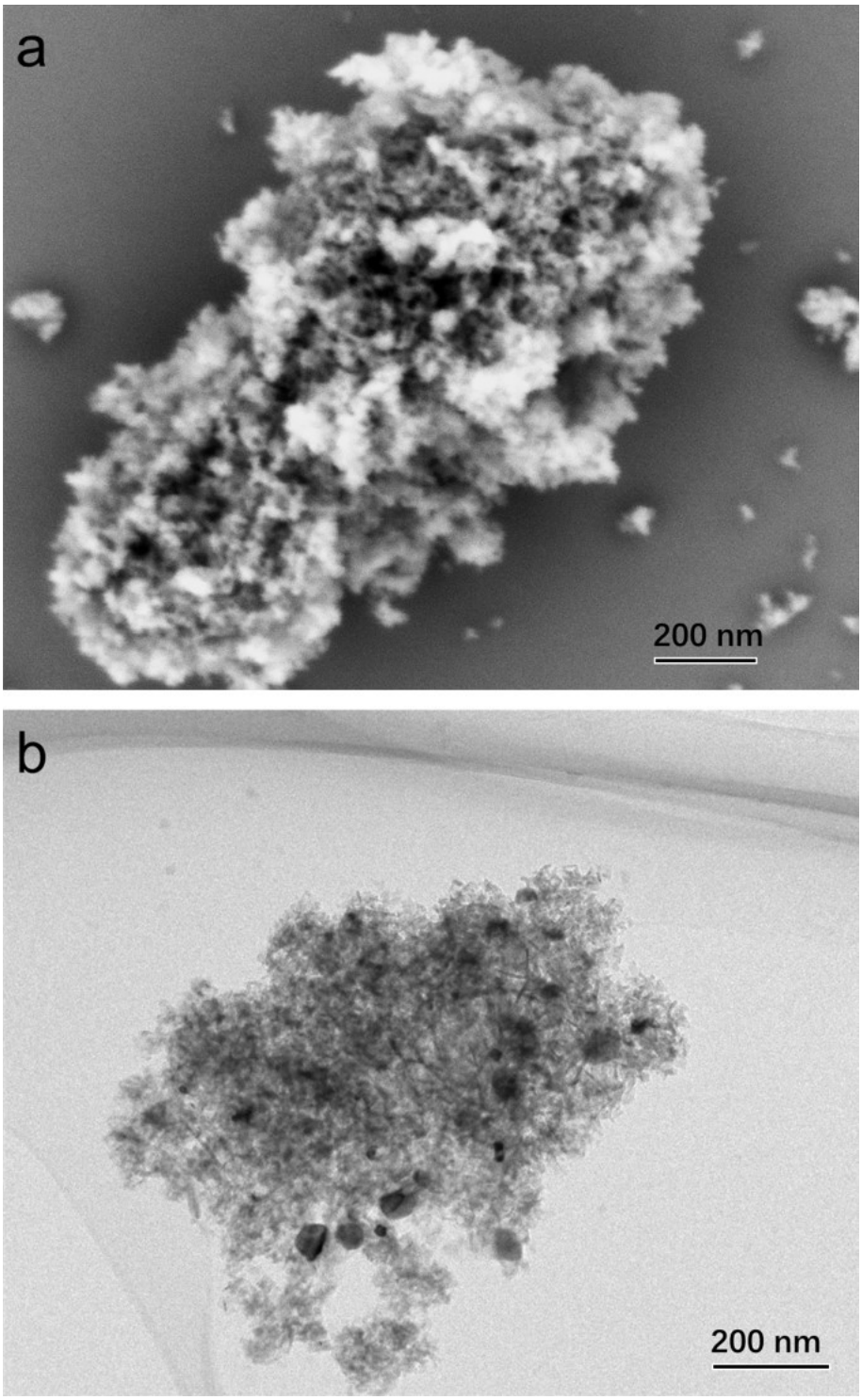

Fig. S6. a SEM image and **b** TEM image of CuO_x&FeO_y/Al_2O_3 after RWGS reaction.

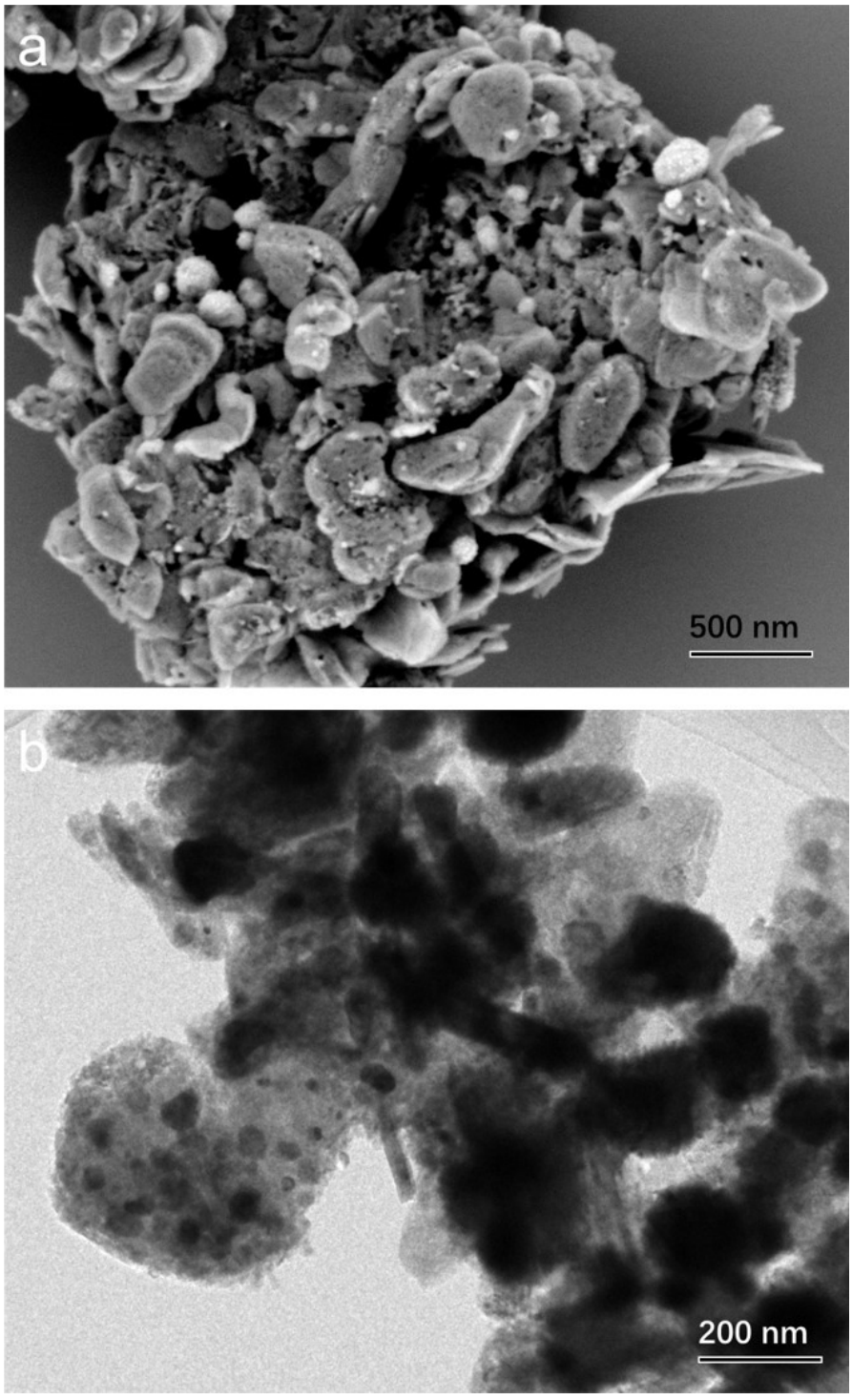

Fig. S7. a SEM image and **b** TEM image of CuO_x&FeO_y/MgO after RWGS reaction.

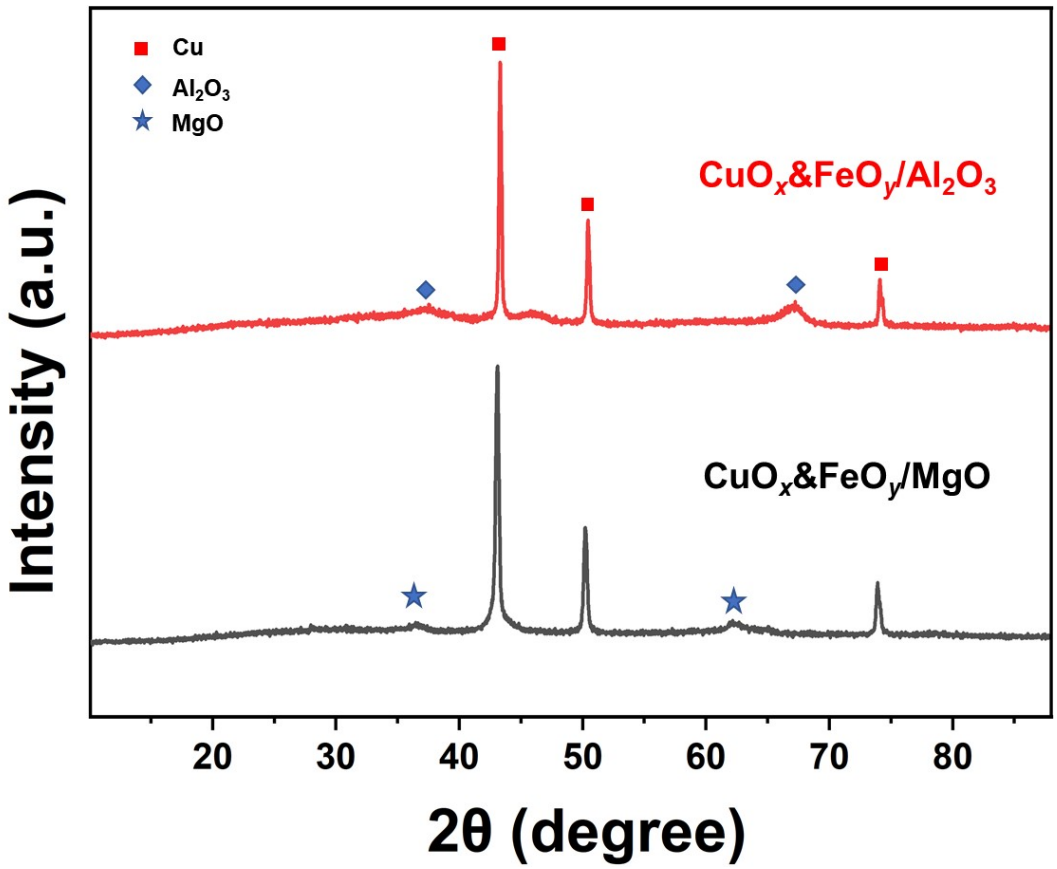

Fig. S8. XRD of CuO_x&FeO_y/Al_2O_3 and CuO_x&FeO_y/MgO after RWGS reaction.

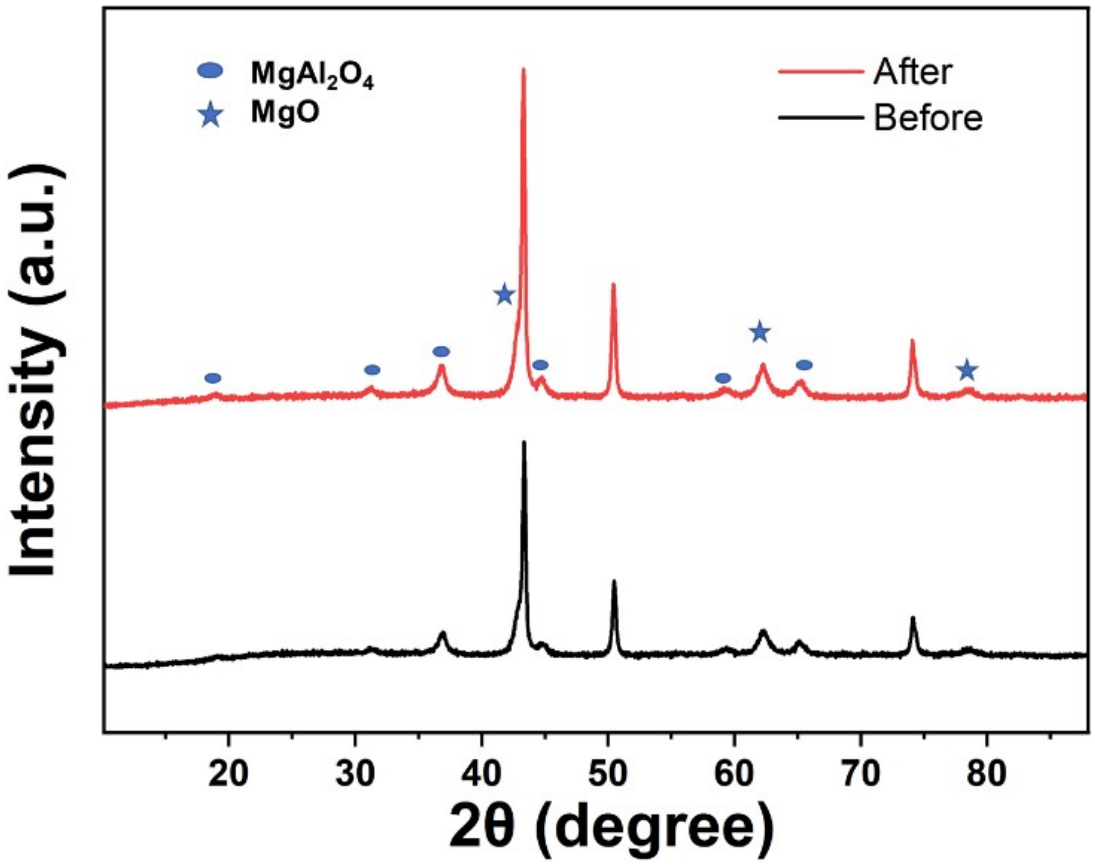

Fig. S9. XRD of T-CuO_x&FeO_y/MAO before and after RWGS reaction.

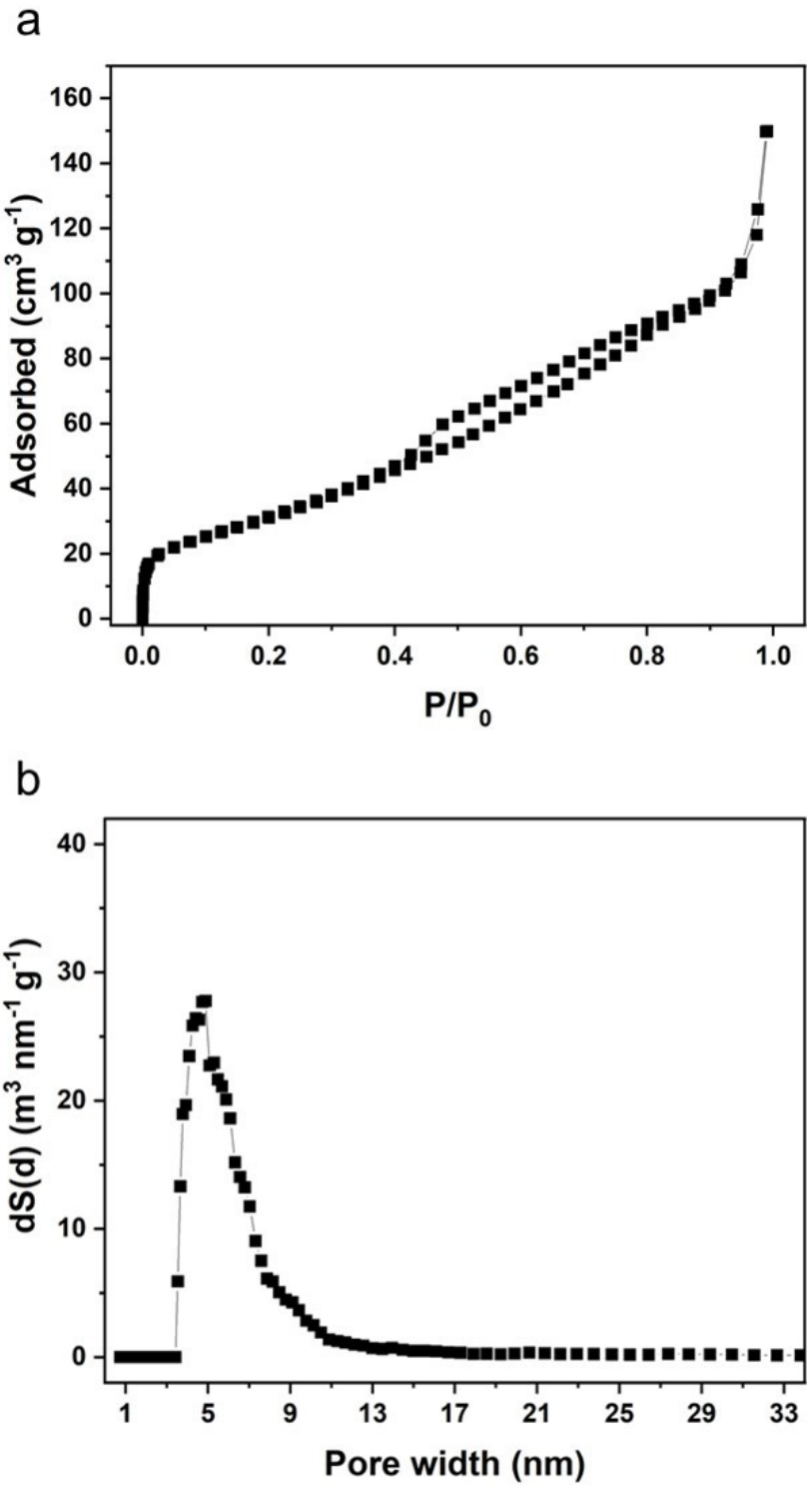

Fig. S10. a Nitrogen adsorption-desorption isotherm and **b** pore-size distribution curve of T-CuO_x&FeO_y/MAO.

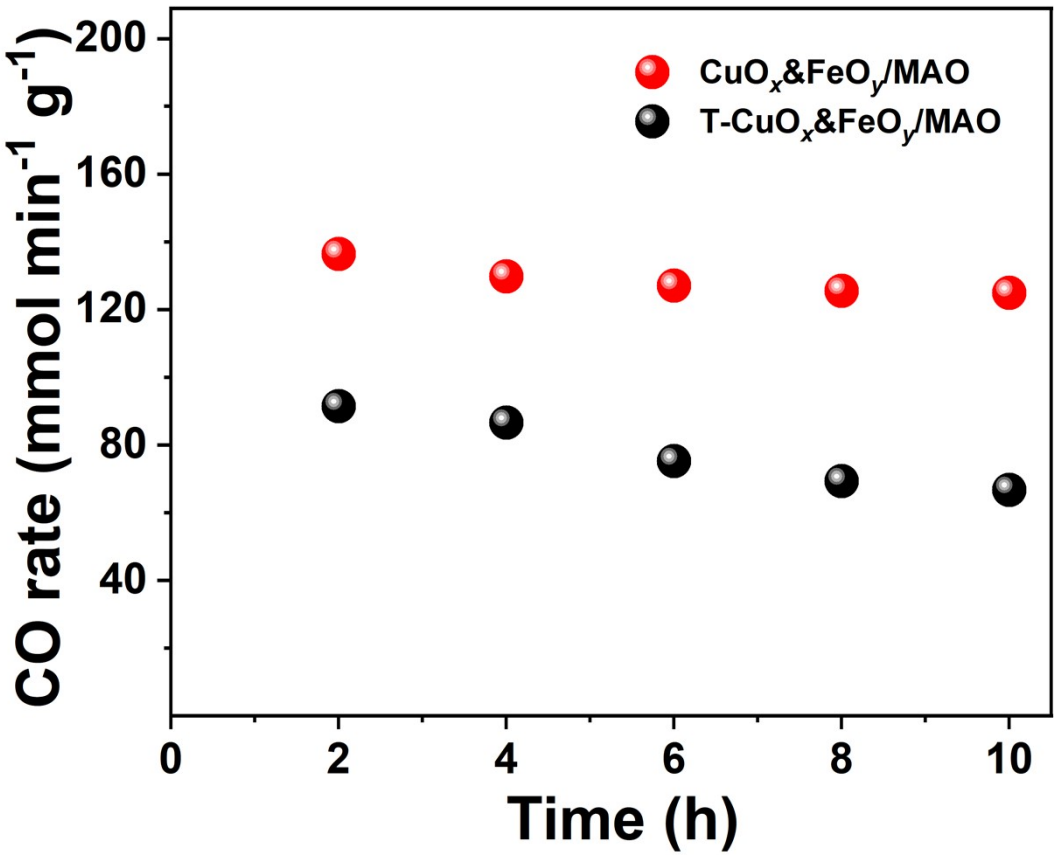

Fig. S11. Catalyst activity measurements of T-CuO_x&FeO_y/MAO.

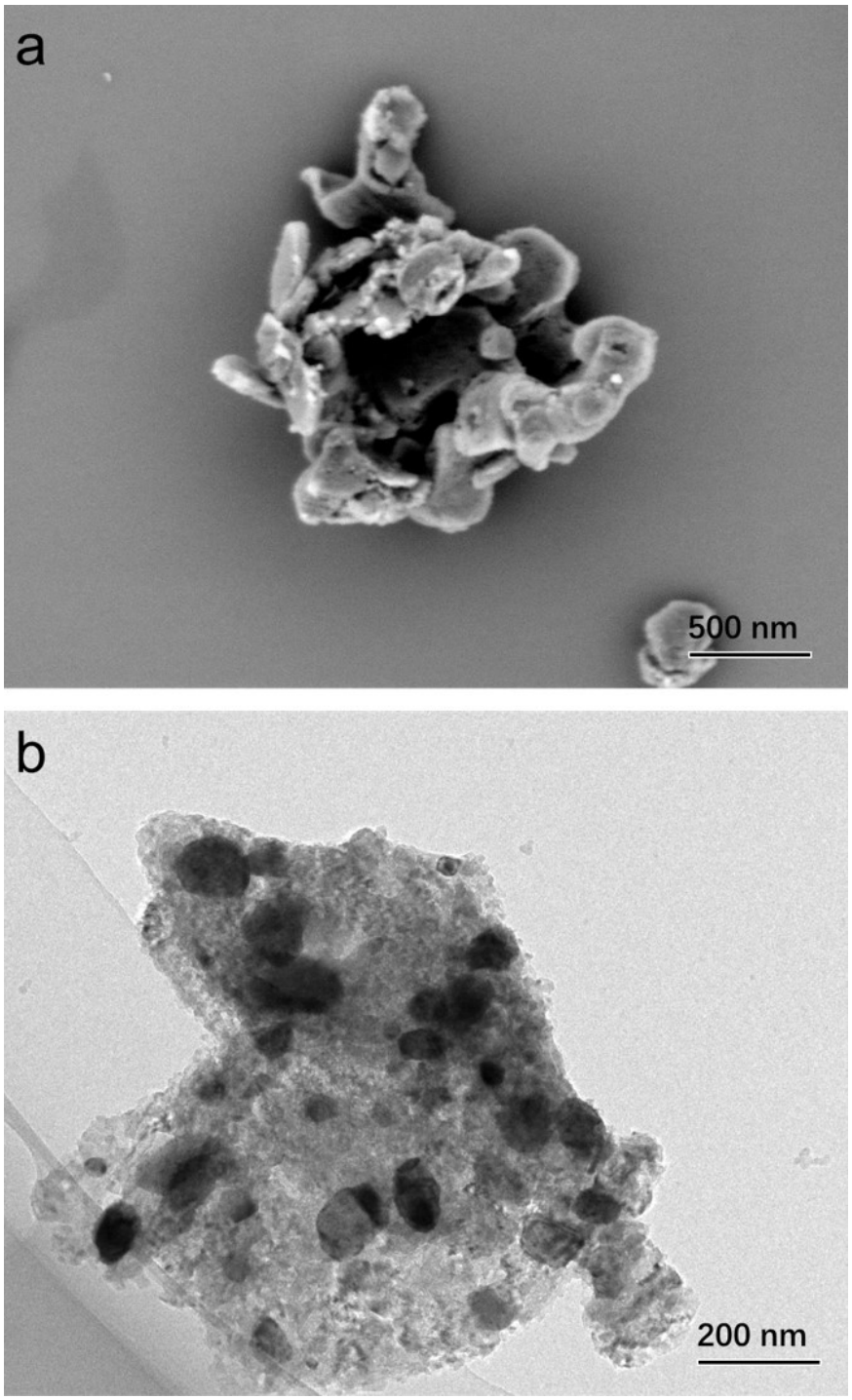

Fig. S12. a SEM image and **b** TEM image of T-CuO_x&FeO_y/MAO after RWGS reaction.

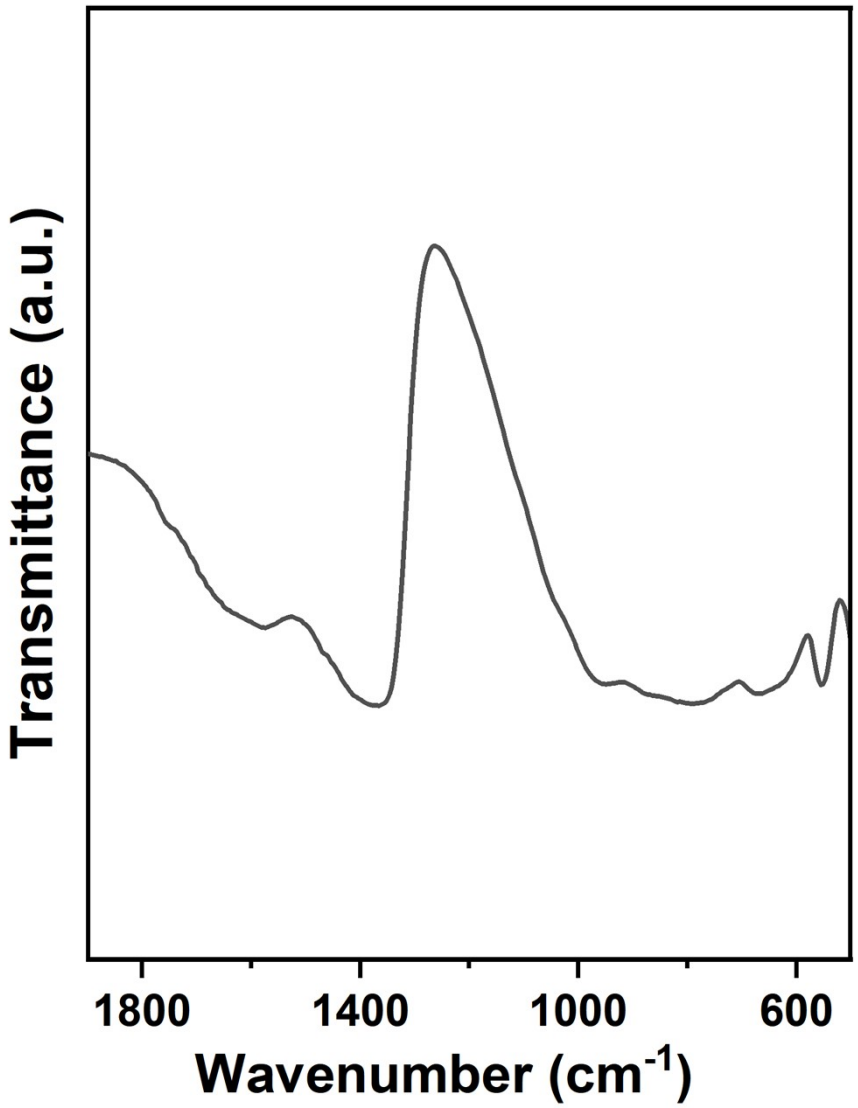

Fig. S13. FT-IR spectrum of LDH.

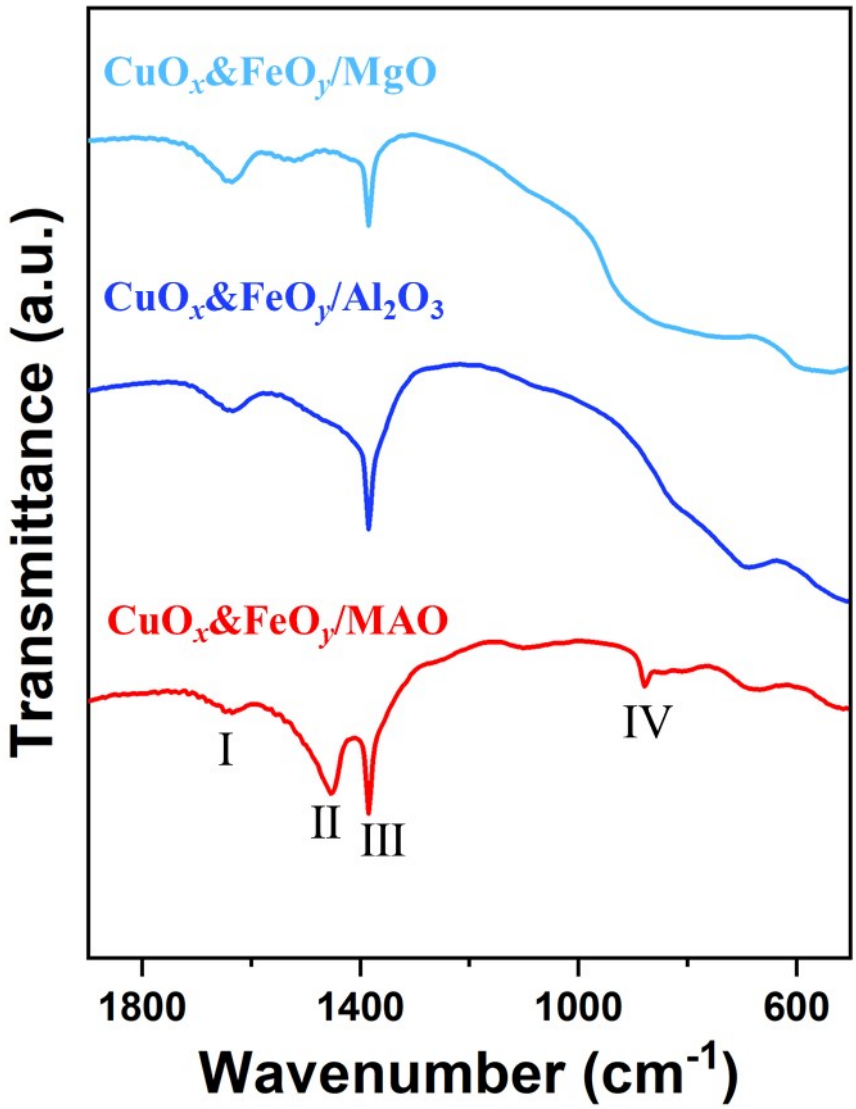

Fig. S14. FT-IR spectrum of the spent catalysts.

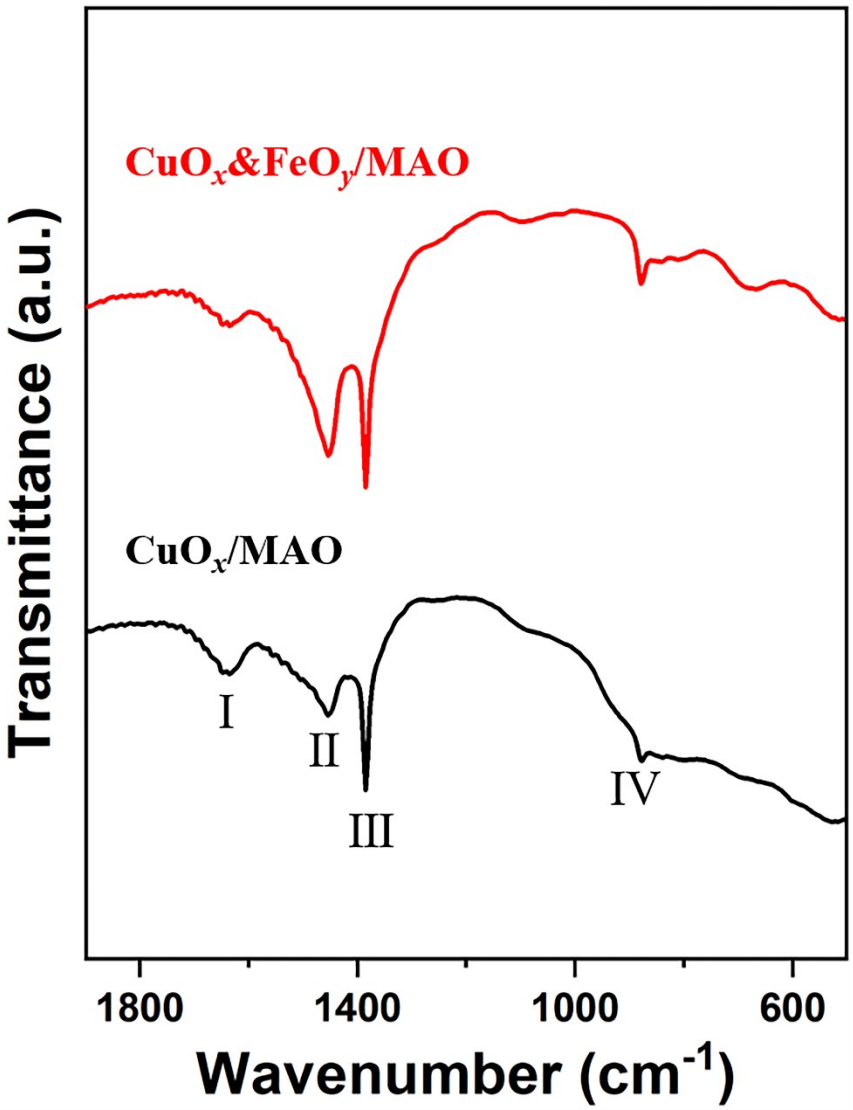

Fig. S15. FT-IR spectrum of the spent CuO_x&FeO_y/MAO catalyst and CuO_x/MAO catalyst.

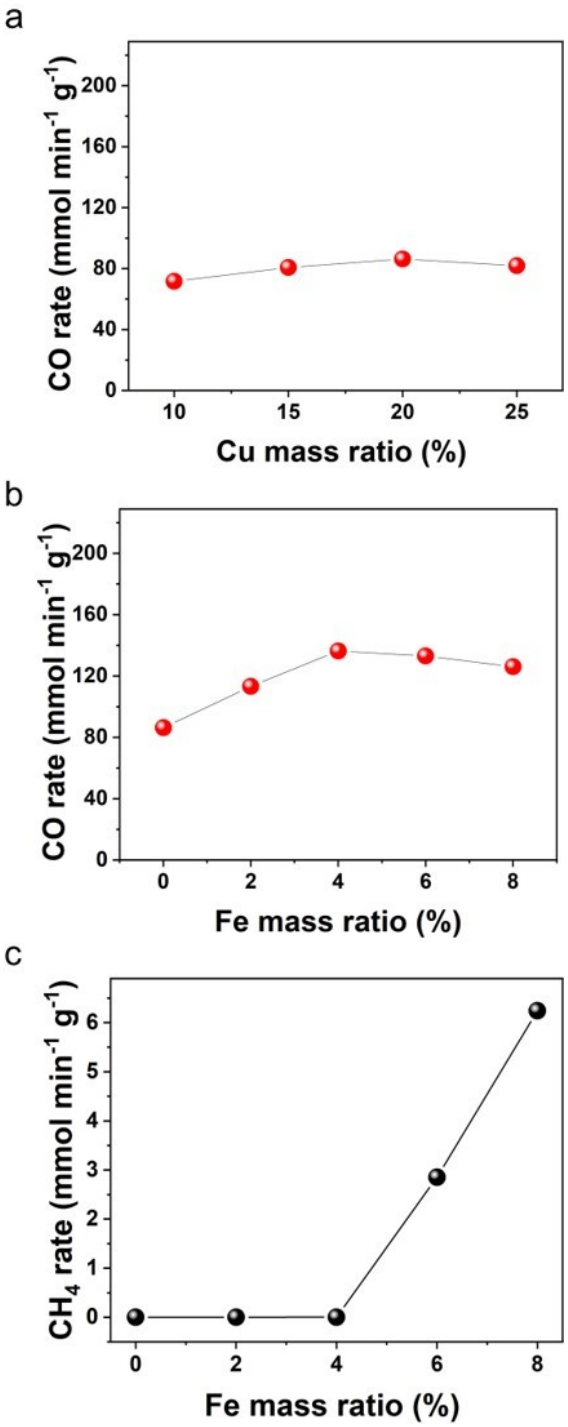

Fig. S16. The effect of catalyst composition on **a**, **b** CO production rate and **c** CH_4 production rate.

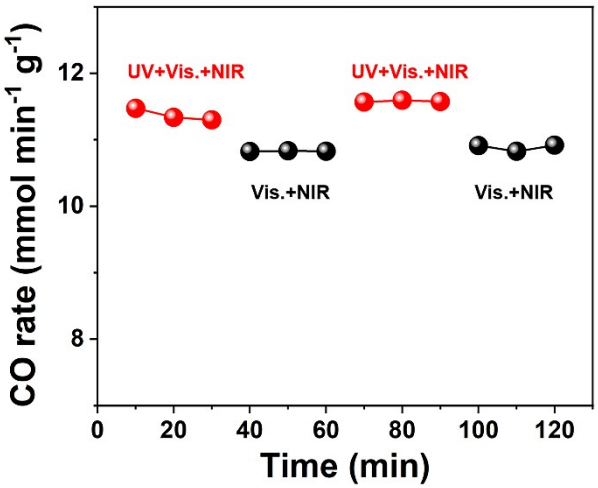

Fig. S17. CO evolution at photothermal condition with and without UV-light illumination over CuO_x&FeO_y/MAO catalyst. 30 mg of the catalyst powder, 376 °C, the total flowrate of H_2 and CO_2 (the molar ratio of H_2: CO_2 = 1: 1) was 60.0 mL min^{-1}.